

## P1.7 OBSERVATIONS OF ICE CRYSTALS AT THE SOUTH POLE USING A CPI AND POLAR NEPHELOMETER

R. Paul Lawson and Qixu Mo  
SPEC Incorporated, Boulder, CO [www.specinc.com](http://www.specinc.com)

### 1. Introduction

SPEC Incorporated collected unique measurements of the size, shape and concentration of over 900,000 ice crystals at the South Pole Station (SPS) during February 2001. This is the first time a statistically large data set of high-definition digital images of ice crystals has been collected in the Antarctic austral summer. In 2001, SPEC operated two cloud particle imagers (CPIs) (Lawson et al. 2001) and in February 2002 added measurements from a polar nephelometer (P-N) (Gayet et al. 1997) that measures scattering phase function.

Detailed measurements of the size, shape and scattering phase function of ice crystals at SPS can be adapted to studies of the optical properties of ice crystals in cirrus and other clouds. The elevation of SPS is about 3.4 km MSL and the temperature in the first 5 km MSL of the atmosphere generally ranges from about  $-32^{\circ}\text{C}$  to  $-40^{\circ}\text{C}$  in February (Warren 1996). Clouds that form in the lower 3 km AGL over the SPS in February often have the appearance of supercooled stratus clouds and cirrus. In the cold atmosphere, ice crystals form in these clouds (and occasionally in cloudless air), fall to the surface and can easily be observed.

The shapes of the ice crystals falling at SPS often appear to be very similar to those observed in cirrus clouds. For example, recent studies using a CPI show that the most common crystal type (by mass) in mid-latitude cirrus is the rosette shape (Lawson et al. 2001; Sassen et al. 2001; Heymsfield et al. 2002). Rosette-shaped crystals were often observed at SPS in 2001 and 2002, probably nucleated in supercooled water clouds (Mahesh et al. 2001), usually within 1 km of the surface. Other crystal habits observed in cirrus, such as columns and plates are also observed at SPS, typically falling from thin, cold clouds that have the same appearance as cirrus.

### 2. Instrumentation

**Figure 1** shows photographs of the CPIs and polar nephelometer installed on the roof of a small building at the SPS. The P-N and the CPI were connected together using a custom-designed plumbing system with inlet funnels to insure particles would pass through the sample volumes of both the CPI and P-N. Constant flow exhaust fans were connected to the exit regions of the CPIs. Before the plumbing system was fabricated out of aluminum, the plumbing system and the sample tubes of the CPI and P-N were constructed using Plexiglas so that flow within the system could be visualized. A fog generator was used to make a cloud that could be visualized using a laser illumination system. **Figure 2** shows a close-up photograph of laser light illuminating the flow through the P-N portion of the plumbing system. The flow visualization tests showed that the sample air reliably passed through both the CPI and P-N viewing areas. The aluminum plumbing was fabricated and the flow rate through the system measured using miniature pitot tubes. **Figure 3** shows the velocity profiles measured in the sample volumes of the CPI and P-N. The measurements show that the velocity profiles in each instrument are relatively flat and that the measurements were repeatable.

At  $33\text{ m s}^{-1}$ , the sample rate of the CPI is  $1.5\text{ L s}^{-1}$ . This sample volume was used to calculate concentrations presented in this work. However, it was observed that the actual sample volume appeared to vary with ambient wind speed and orientation of the CPI. This was determined qualitatively by moving the orientation of the CPI, measuring crystal concentration and returning the CPI to its original position. Since there was no way to make quantitative measurements of the uncertainty in particle flow rate, we cannot quote uncertainties in ice crystal concentration measurements. However, the shape of the particle size distributions should not be affected, only the total crystal concentration. The CPIs were generally operated about 12 to 18 hours per

---

\* *Corresponding Author Address:* Dr. R. Paul Lawson, SPEC Incorporated, 3022 Sterling Circle, Boulder, CO. 80301; email: [plawson@specinc.com](mailto:plawson@specinc.com)

day, unless an instrument was shut down due to electrical outages or other interruptions at SPS.



**Figure 1.** Photographs of the SPEC CPIs and LaMP Polar Nephelometer (P-N) on top of a small building at the South Pole. The P-N is seen connected to the exhaust region of the CPI in the panel at the upper left. Both instruments are aspirated using an exhaust fan. The sampling elevation is about 3 m.

There are several *advantages* to collecting data with a CPI over previous studies that captured ice crystals on glass slides and then photographed them under a microscope (e.g., Shimizu 1963; Kikuchi 1970; Hogan 1975; Kikuchi and Hogan 1978; Ohtake and Yogi 1979; Ohtake and Inoue 1980; Smiley et al. 1980; Inoue et al. 1984; Tape 1994), which is a tedious and slow process. The primary advantages of using the CPI are: *First*, the CPI records ice crystal images at a high rate (up to several tens per second) and can

run unattended, producing a very large data set compared to previous techniques; *Second*, the images can be processed using software that automatically determines crystal dimensions, area, perimeter, fractal dimension and mass, and classifies crystal type; and *Third*, the large data set that is collected can be analyzed to produce meaningful classifications of the frequency of particle types and correlations with ambient conditions.

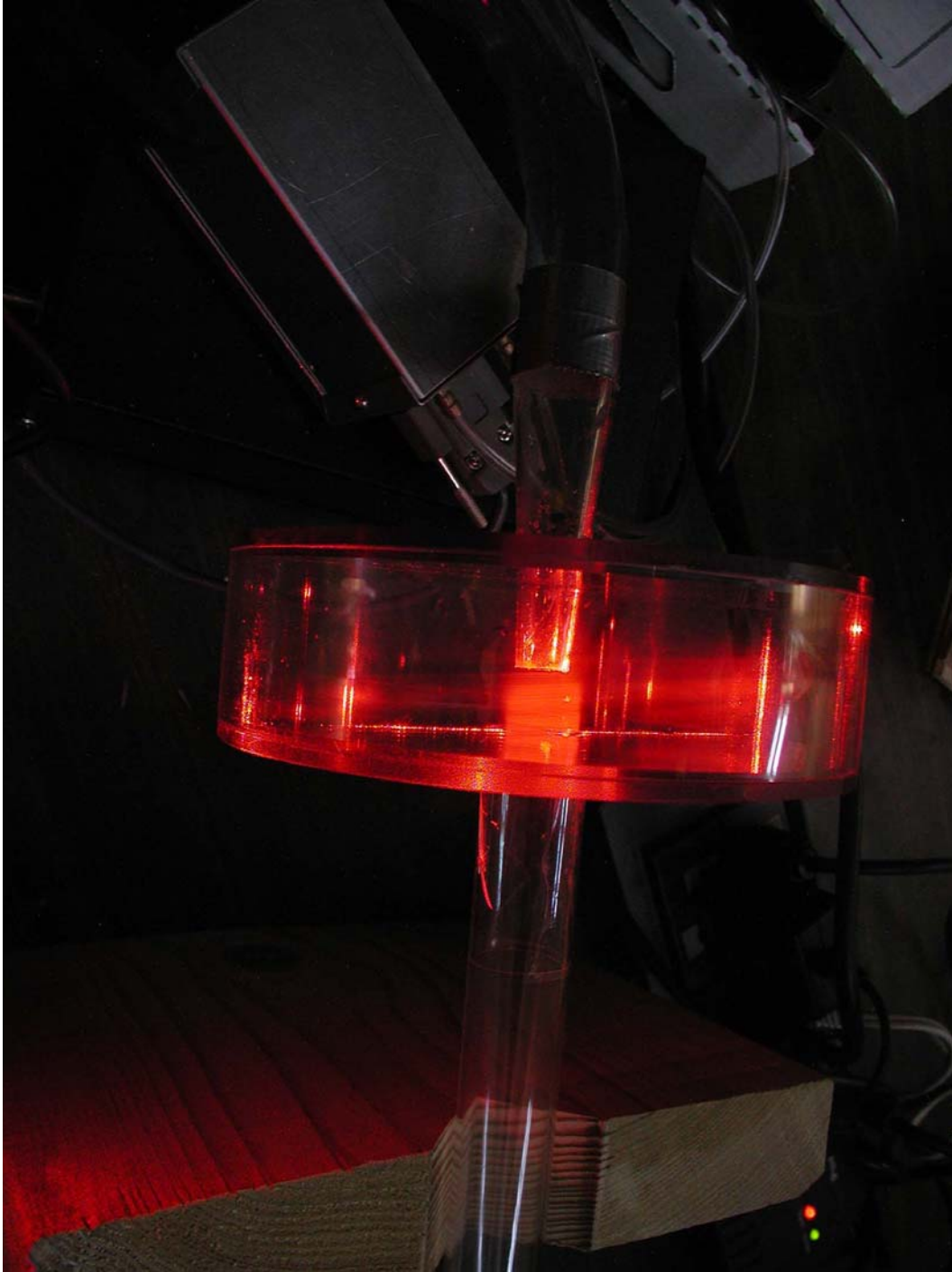


**Figure 2.** Photograph showing a portion of the Plexiglas tubing and P-N sample area with fog drops illuminated by laser light. The Plexiglas tubing was used to simulate the aluminum plumbing system fabricated to connect the sample areas of the CPI and P-N.

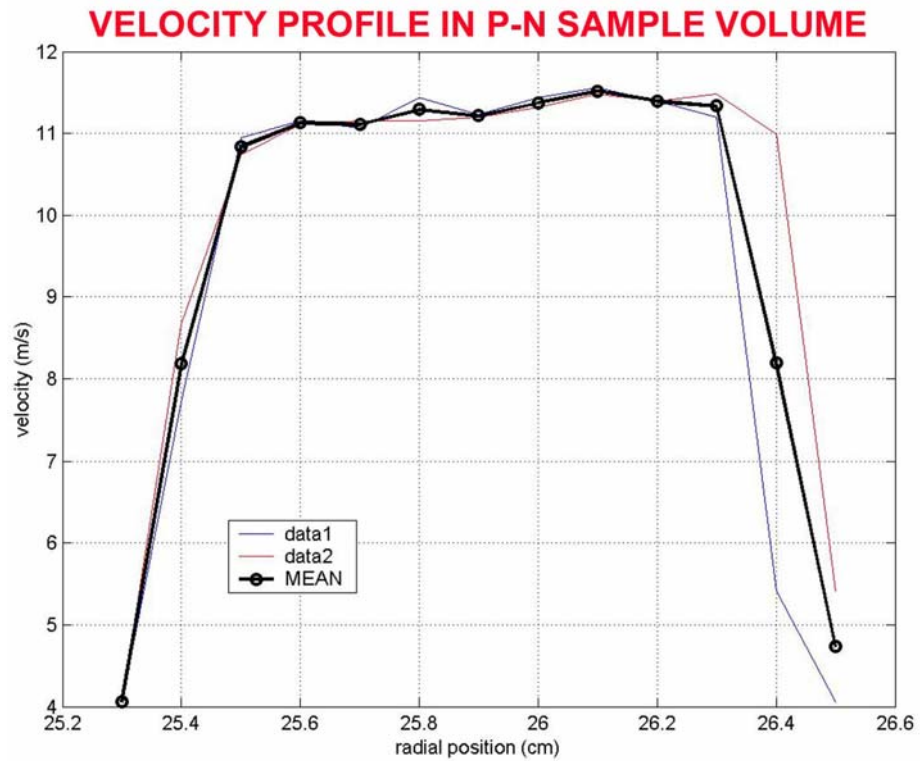
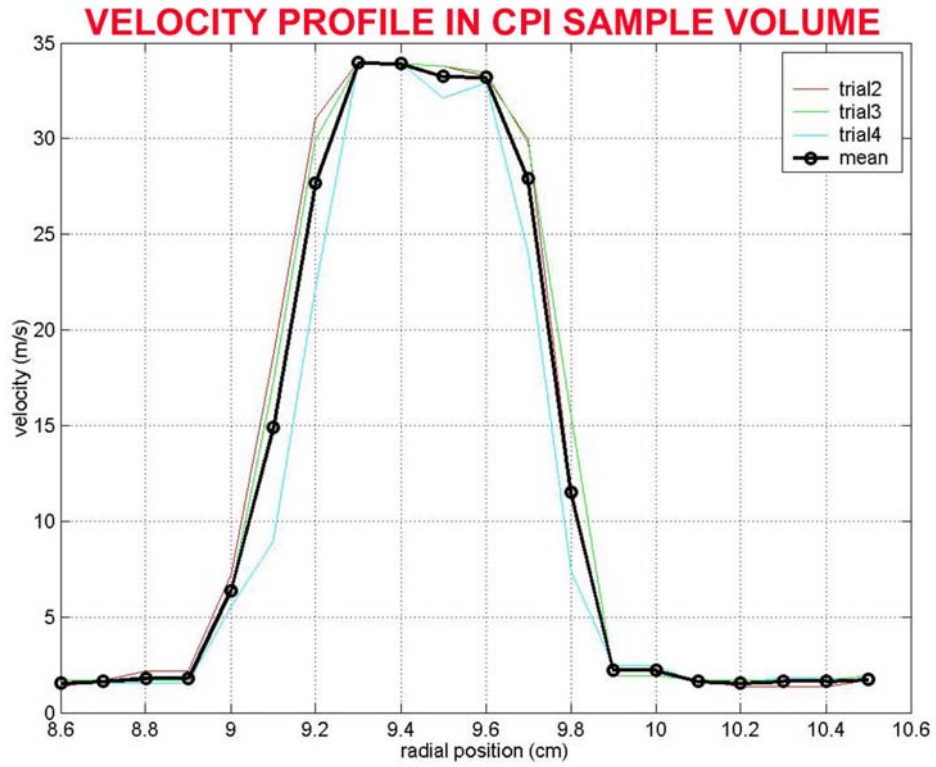


**Figure 3.** Velocity profiles measured in the CPI and P-N sample volumes with plumbing connecting the two instruments as shown in **Figure 1**.

### 3. Data Collection

#### 3.1 Results of Crystal Habit Classification from 2001

A total of 901,595 CPI images of ice crystals from the period 1 – 8 February 2001 were placed into categories using an automatic crystal habit classification program. On occasion, the automatic crystal classification program could not distinguish reliably between crystal types (e.g., distinguishing irregulars from thick plates; columns from single bullets). When this occurred, which was in about 20% of the data set, the crystals were visually classified. The overall accuracy of crystal classifications shown is estimated to be < 10%. However, it should be kept in mind that even visual classification of crystal habits is subjective.

During the 1 – 8 February period, the surface temperature at SPS ranged from –30 to –39° C. Of the total, 180,023 crystal images smaller than 50  $\mu\text{m}$  were eliminated, because the program could not reliably distinguish between small spheroids, irregular shapes and small plates. **Figure 4** shows a histogram of the percentage breakdown of the remaining 721,572 crystals > 50  $\mu\text{m}$ . The histogram is shown as a function of particle number, area and mass for eight habit categories. **Figure 5** shows typical examples of CPI images classified in **Figure 4**, along with an example of CPI images smaller than 50  $\mu\text{m}$  that were excluded from the histogram. Crystals classified as short columns/thick plates (C1g in the Magono and Lee 1966 classification), columns (C1e and C1f) and plates (P1a) are also labeled “diamond dust” in **Figure 4**, due to their sparkly appearance in sunlight. As discussed later, diamond dust is typically observed under very thin high clouds that are penetrated by the sun’s rays and often produce optical effects, such as halos and arcs (Tape 1994).

Crystals classified as rosettes, budding rosettes (rosettes with short branches), complex crystals, which are rosette shapes with side planes, fall into a general category we will call rosette shapes. Single bullets were rarely observed and were always associated with rosette shapes. The rosette shapes are polycrystals that are typically formed from rapid freezing of a supercooled drop or haze particle (Pruppacher and Klett 1997; Bacon et al. 2002). Bailey and Hallett (2004) found that rosette-shaped polycrystals are grown in the laboratory when temperatures are between about -30 and -70° C.

They also observed that bullet rosettes, which they define as a distinct class of rosette-shaped crystal without side plane or irregular branches, are only observed at temperatures < -40°C. Bailey and Hallett found that rosette shapes with side plane predominate at temperatures between about –30 and –40 ° C, which is in general agreement with our observations at SPS.

In addition to the general classifications of diamond dust and rosette shapes, the other major category shown in **Figure 4** is irregular shaped crystals. Korolev et al. (1999) found that non-pristine shaped ice crystals accounted for > 95% of the shapes observed in Arctic ice clouds. Our observations suggest that non-pristine shapes are not nearly as prevalent in precipitating Antarctic clouds, but contamination from blowing snow makes it impossible to make a quantitative assessment. The irregulars observed at SPS were usually small (< ~100  $\mu\text{m}$ ) ice particles. Irregulars in blowing snow were observed when there were no precipitating crystals, and irregular crystals were observed when the wind was too weak to generate blowing snow. The only discernable difference, which is not absolutely distinctive, is that the blowing snow irregulars generally had more rounded edges (**Figure 5**). It was not possible to determine the percentage of blowing snow from precipitating irregular crystals. However, for more than 80% of the time during 1 – 8 February 2001, the wind was in excess of 4  $\text{m s}^{-1}$ , which was typically the threshold wind speed for generating blowing snow during this period.

When sorted by number, diamond dust (columns, thick plates and plates) constitute 45% of the crystals, rosette shapes 30% and irregulars 25%. However, when sorted by area, rosette shapes comprise 50%, diamond dust 30% and irregulars 20%. By mass, the percentages are 57% rosette shapes, 23% diamond dust and 20% irregulars. Thus, the rosette shapes, while less frequent in occurrence, accounted for the majority of the area and mass of ice crystals observed at SPS during 1 – 8 February.

A time-series showing the concentration and habits of ice crystals > 50  $\mu\text{m}$  observed at SPS when the CPI was operating from 1 – 8 February 2001 is shown in **Figure 6**. During the observation period, the environmental conditions associated with generation of diamond dust were, for the most part, exclusive of the conditions that supported production of rosette shapes. Typically, rosette shapes were observed when

there was a broken or overcast layer within about 1 km of the surface. Since polycrystalline crystals, such as bullet rosettes, are thought to form when a supercooled water drop freezes rapidly, it is likely that these clouds contained water drops. Support for this premise at SPS comes from additional observations conducted by Mahesh et al. (2001). They observed supercooled liquid water drops in the temperature range from -28°C to -35°C using a HiVis balloon-borne sonde,

which records video images of cloud particles (Orikasa and Murakami 1997). Diamond dust was typically observed when there were high, thin clouds, often with atmospheric optics and the sun visible through the clouds. Generally, very few or no crystals were observed when there were no clouds, which is in general agreement with findings from other investigators (see for example, Bromwich 1988).

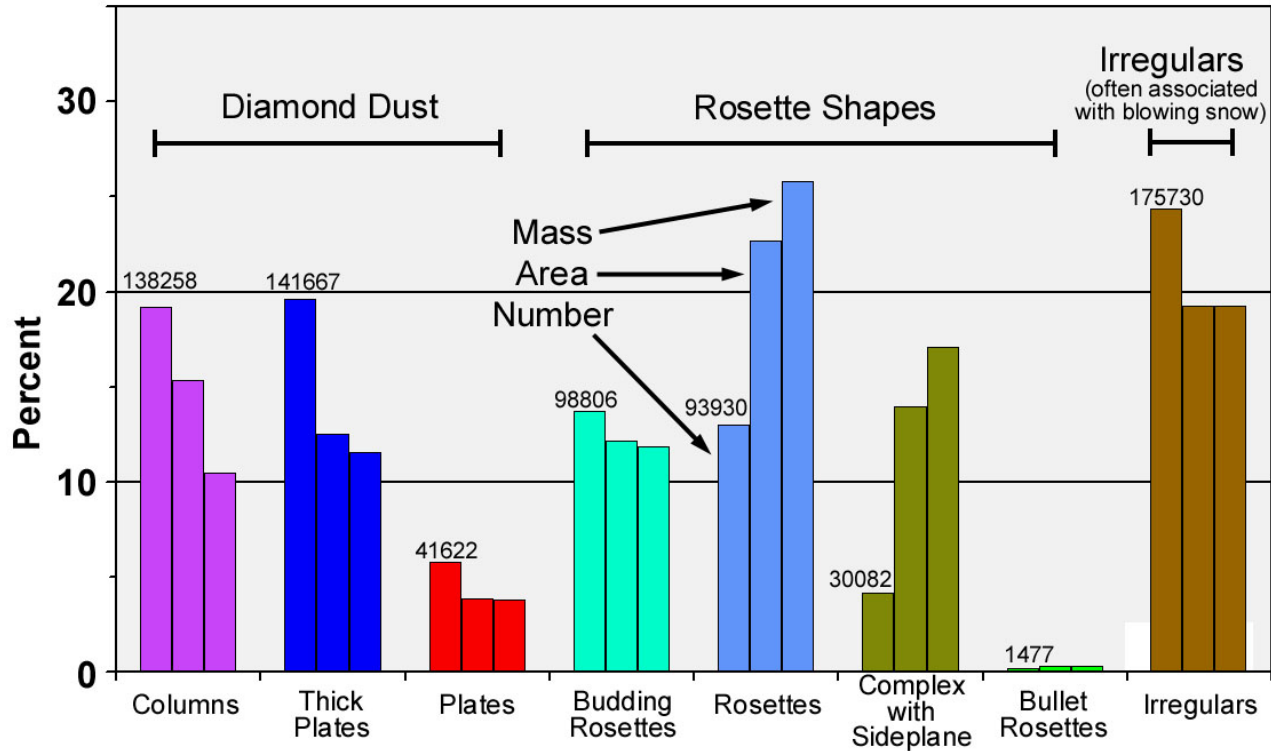


**Figure 4.** Histogram of ice crystal habits observed at SPS during the period 1 – 8 February 2001. The percentage weighted by concentration, area and mass is shown for each habit category. Columns, thick plates/short columns and plates are associated with diamond dust. Budding rosettes, rosettes and complex with side plane are associates with rosette shapes. The total number of crystals of each habit is shown above its category. The total number of ice crystals categorized is 721,572.

**Figure 7** shows an example on 1 February 2001 during a period when there was diamond dust, and another example on 3 February 2001 when there were rosette shapes. For reference, each of the periods is also highlighted in **Figure 6**. The cloud cover, also shown on **Figure 7**, was relatively thin and high (4,000 ft AGL) on 1 February, and low (1,000 ft AGL) and overcast on 3 February. The cloud cover is derived from routine hourly observations taken by NOAA meteorologists at SPS, and when an hourly observation is missing, the data are supplemented

by observations from SPEC scientists and measurements from the NASA vertically-pointing micro pulse lidar (Campbell et al. 2002), based at the NOAA Atmospheric Research Observatory (ARO) at SPS. Below the cloud cover, **Figure 7** shows examples of CPI images observed in each of the two regimes. The diamond dust is composed of mostly pristine crystals, consisting of mostly thick plates/short columns, long columns and clear plates. The rosettes shapes are mainly bullet rosettes and budding rosettes, i.e., rosettes with short arms.

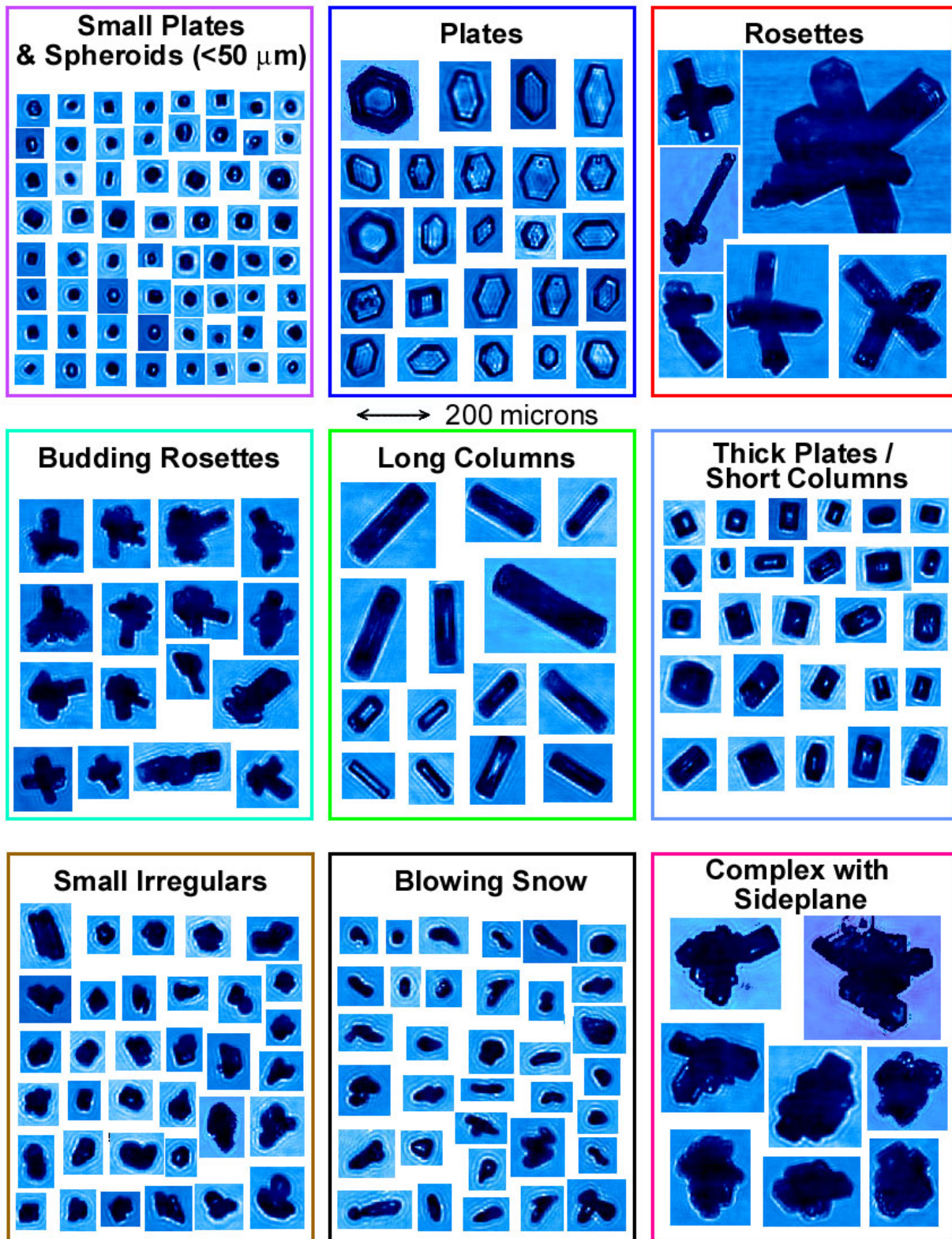
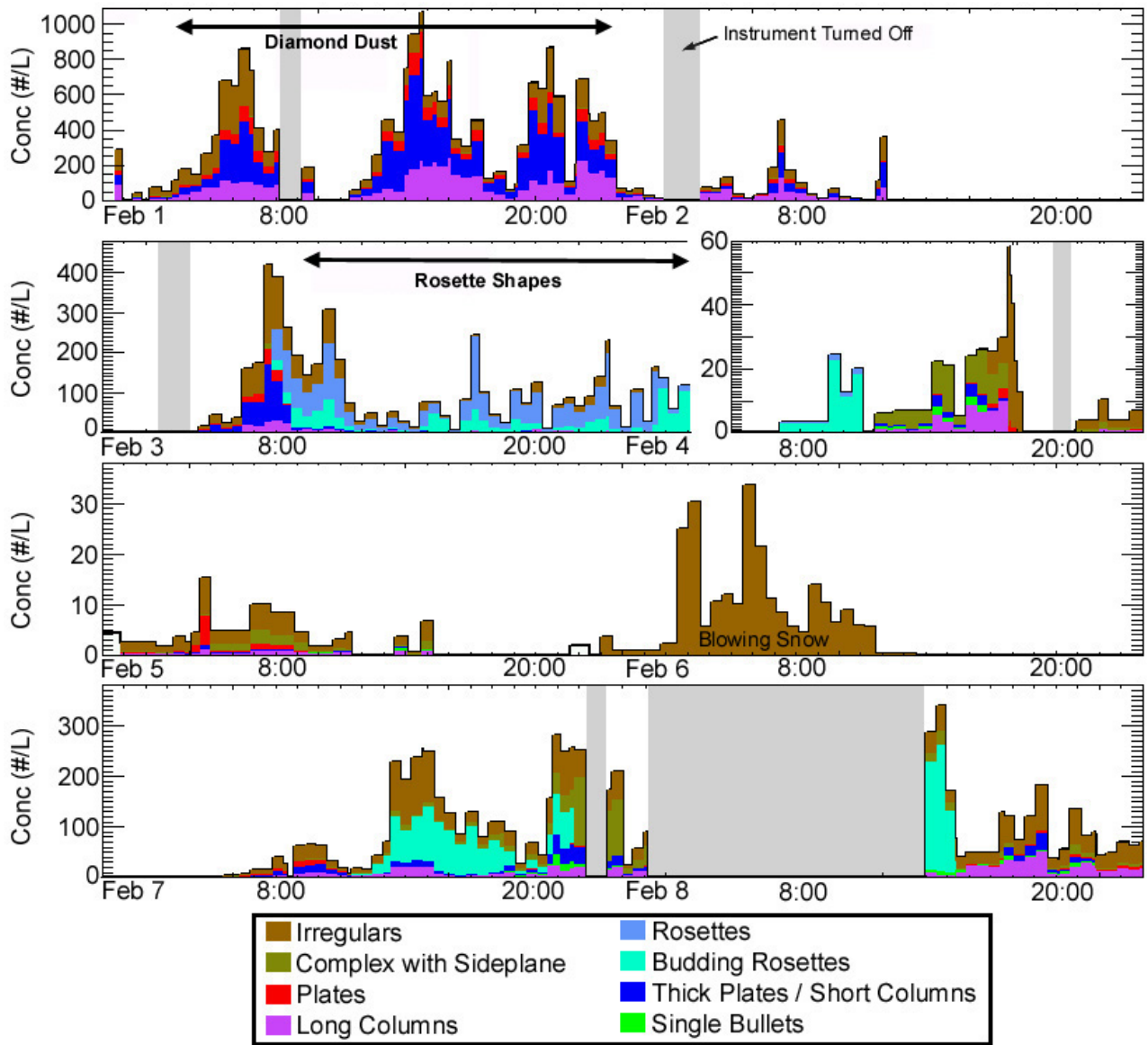
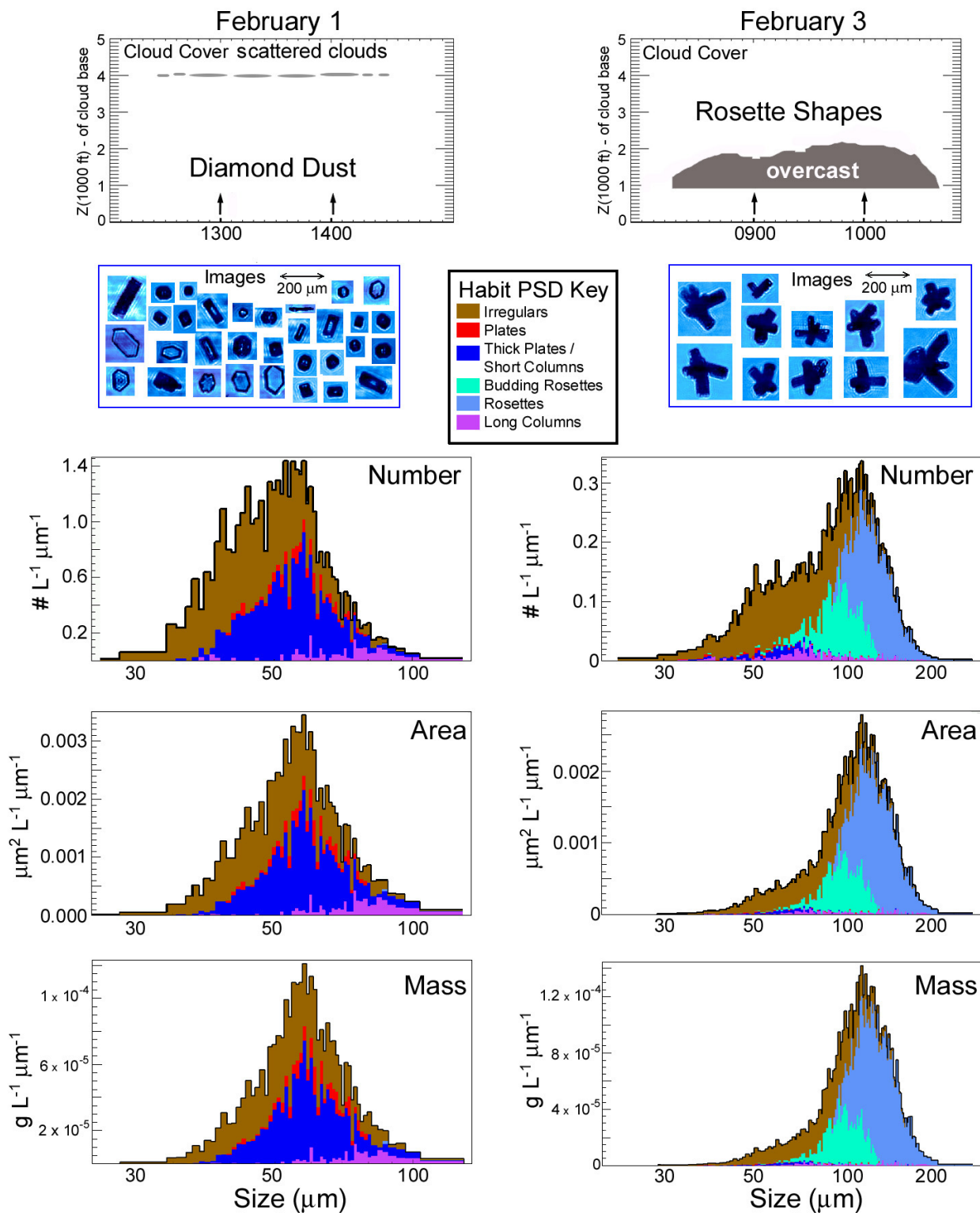


Figure 5. Examples of CPI images of ice crystals sorted into habit categories.



**Figure 6.** Time series showing CPI measurements of 721,572 ice crystals  $> 50 \mu\text{m}$  observed at SPS during the period 1 – 8 February 2001. Total ice crystal concentration is shown on the ordinate and ice crystal habits are color coded. A period with “diamond dust” on 1 February and a period with “rosette shaped” ice crystals on 3 February are shown in more detail in **Figure 7**.



**Figure 7.** Example of time periods (shown in **Figure 6**) when (left) diamond dust and (right) rosette shapes are prevalent. Elevation and type of cloud cover is shown in the top panels, examples of CPI images are shown below cloud cover, and PSDs weighted by concentration, area and mass, and color-coded to show crystal habits are shown in the bottom three panels.

**Figure 7** also shows particle size distributions (PSDs), including crystals  $< 50 \mu\text{m}$ , weighted by concentration, area and mass. The PSDs in **Figure 7** are also color-coded to show the relationship between crystal habits and size. The crystals  $< 50 \mu\text{m}$  in PSDs representing both diamond dust and rosette shapes have been lumped together into a category called small spheroids and plates and called irregulars  $< 50 \mu\text{m}$  (see examples of CPI images in **Figure 5**). It is not possible to sort these small crystals into categories using the automated classification program. However, visual inspection of the images shows that when diamond is observed, there is a much higher percentage of small plates, and when rosette shapes are observed, there is a much higher percentage of small spheroids. This is expected (Pruppacher and Klett 1997; Bacon et al. 2002), since diamond dust (i.e., hex shape) is expected to grow via vapor diffusion after heterogeneous nucleation, and rosettes are generally formed by rapid freezing of a supercooled drop (i.e., spheroidal shape).

The PSDs in **Figure 7** show that the diamond dust extends out to sizes of about  $150 \mu\text{m}$  and is dominated by thick plates with some columns and plates, and that rosette shapes extend out to about  $250 \mu\text{m}$ . These larger sizes can be expected due to their formation and growth in a water-saturated environment. From  $50$  to  $80 \mu\text{m}$ , the rosette-shapes PSD consists of mostly irregulars, along with a small percentage of thick plates/ short and long columns. From  $80$  to about  $130 \mu\text{m}$ , budding rosettes dominate the PSD, and rosettes predominate from  $130$  to  $250 \mu\text{m}$ . About 80% of the mass of ice crystals  $> 80 \mu\text{m}$  consists of budding rosettes and rosettes.

### 3.2 Results of Optical Effects Observed in 2002

As shown in **Figure 1**, one of the CPIs was connected in tandem with a polar nephelometer developed by the French Laboratoire de Meteorologie Physique (LaMP) (Gayet et al. 1997; Crepel et al. 1997). The LaMP polar nephelometer (P-N) has been used to measure scattering phase function at the surface and from an aircraft (Oshchepkov et al. 2000; Gayet et al. 1998). Tape (1994) found that visual halos are observed at the SPS station during conditions when pristine columns and/or plates are present. We found that  $22^\circ$  and  $46^\circ$  halos corresponding

to visual observations were only measured by the P-N when the CPI recorded relatively low concentrations of pristine columns and plates, and that no visual halos were observed in overcast conditions when rosettes were precipitating.

**Figure 8** shows an example of a comparison of ice crystals observed by the CPI and phase function measurements measured by the P-N during conditions when atmospheric halos were and were not observed. The  $22^\circ$  and  $46^\circ$  halos are observed when there was a low concentration of pristine diamond dust ice crystals, while flat, featureless phase functions were observed when rosettes shapes were present.

### 4.0 Summary

Over 900,000 ice crystals were imaged by CPIs during the period 1 – 8 February 2001 when the surface temperature ranged from  $-30$  to  $-39^\circ\text{C}$ . Of these, 721,572 CPI images were  $> 50 \mu\text{m}$  and sorted into habit categories. Pristine “diamond dust” ice crystals were usually observed with sizes  $< \sim 150 \mu\text{m}$  and consisted of thick plates/short columns, columns and plates. Diamond dust was typically associated with thin, relatively high (1 to 2 km) clouds. The sun was usually visible through these clouds and optical effects were often observed. Budding rosettes, rosettes and complex shapes with side plane were lumped into a category called “rosette shapes”, which were typically  $< \sim 250 \mu\text{m}$  in size and were observed under low ( $< 1$  km) overcast clouds. Limited balloon observations (Mahesh et al. 2001) showed that these clouds contained supercooled liquid water at temperatures between  $-25$  and  $-35^\circ\text{C}$ .

When sorted by number, diamond dust (columns, thick plates and plates) constitute 45% of the crystals, rosette shapes 30% and irregulars 25%. When sorted by area, rosette shapes comprise 50%, diamond dust 30% and irregulars 20%. By mass, the percentages are 57% rosette shapes, 23% diamond dust and 20% irregulars. Thus, the rosette shapes, while less frequent in occurrence, accounted for the majority of the area and mass of ice crystals observed at SPS during 1 to 8 February.

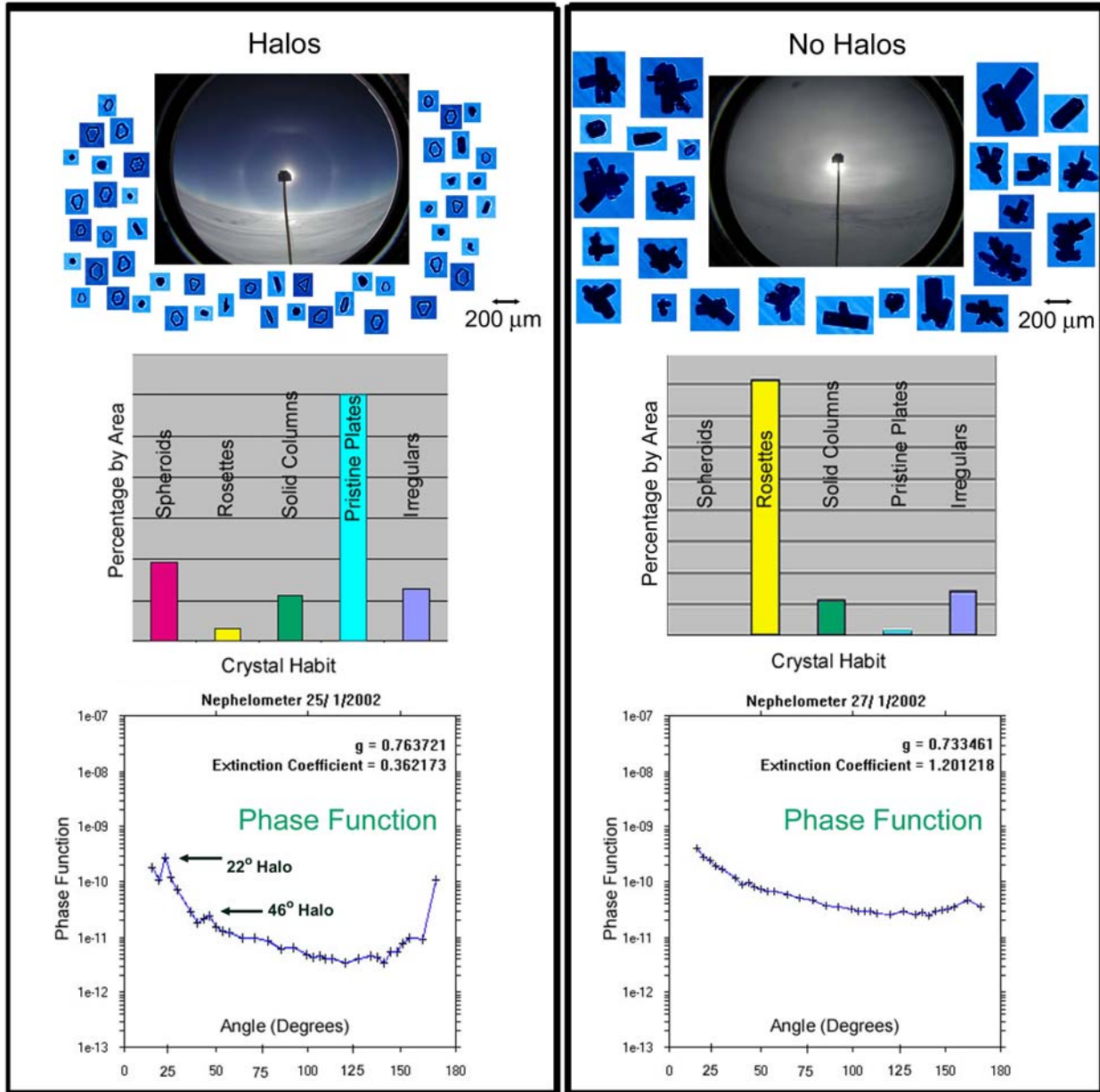


**Figure 8.** Examples of sky cover, CPI images of ice crystals and measured phase functions during a period with (left) Diamond Dust ice crystals, and (right) Rosette Shaped ice crystals observed at SPS in February 2002.

Irregular shaped ice crystals were observed at SPS in all types of falling precipitation and in blowing snow, which was prevalent when the wind speed is  $> \sim 4 \text{ m s}^{-1}$ . Irregular ice crystals in blowing snow were observed to generally have more rounded edges than irregulars in precipitation.

In February 2002, SPEC added a polar nephelometer in tandem with one of the CPIs, in order to make measurements of scattering phase

function. Preliminary results from these measurements show that 22°C and 46°C halos were associated with low concentrations of diamond dust ice crystals with the sun shining through thin, high, scattered clouds. The halos were observed visually and in the phase functions measured by the polar nephelometer. Atmospheric halos were not seen when rosette shaped ice particles were observed falling from a low, thick overcast cloud.

## 5.0 References

- Bacon, N. J., Baker, M. B. and B. D. Swanson, 2003: Initial stages in the morphological evolution of vapour-grown ice crystals: A laboratory investigation. *Quart. J. Roy. Meteor. Soc.*, **129**, 1903-1927.
- Bailey, M. and J. Hallett, 2004: Growth rates and habits of ice crystals between  $-20^{\circ}$  and  $-70^{\circ}$  C. *Quart. J. Roy. Meteor. Soc.*, **61**, 514-544.
- Bromwich, D.H., 1988: Snowfall in high southern latitudes. *Rev. of Geophys.*, **26**, 146-168.
- Campbell, J.R., D.L. Hlavka, E.J. Welton, C.J. Flynn, D.D. Turner, J.D. Spinhirne, V.S. Scott, and I.H. Hwang, 2002: Full-time, eye-safe cloud and aerosol lidar observation at atmospheric radiation measurement program sites: Instrument and data processing." *J. Atmos. Oceanic Technol.*, **19**, 431-442.
- Crépel, O., J-F Gayet, J-F Fournol and S. Oshchepkov, 1997: A new airborne polar nephelometer for the measurements of optical and microphysical cloud properties. Part II: Preliminary tests. *Annales Geophysicae*, **15**, 4, 460-470 (Springer-Verlag).
- Gayet, J-F, O. Crépel, J-F Fournol and S. Oshchepkov, 1997: A new airborne polar nephelometer for the measurements of optical and microphysical cloud properties. Part I: Theoretical design. *Annales Geophysicae*, **15**, 451-459.
- Gayet, J.-F., F. Auriol, S. Oshchepkov, F. Schröder, C. Duroure, G. Febvre, J.-F. Fournol, O. Crépel, P. Personne and D. Daugereon, 1998: In situ measurements of the scattering phase function of stratocumulus, contrails, and cirrus. *Geophys. Res. Letters*, **25**, 7, 971-974.
- Heymsfield, A.J., S. Lewis, A. Bansemer, J. Iaquinta, L.M. Miloshevich, M. Kajikawa, C. Twohy and M.R. Poellot, 2002: A general approach for deriving the properties of cirrus and stratiform ice cloud particles. *J. Atmos. Sci.*, **59**, 3-29.
- Hogan, W.H., 1975: Summer ice crystal precipitation at the South Pole. *J. Appl. Meteorol.*, **14**, 246-249.
- Inoue, M. T. Ohtake and G. Wakahama, 1984: Summer precipitation onto the south polar plateau. *Mem. Nat'l. Inst. Polar Res. Special Issue Jpn*, **34**, 70-86.
- Kikuchi, K., 1970: Peculiar shapes of solid precipitation observed at Syowa Station, Antarctica. *J. Met. Soc. Japan*, **48**, 243-249.
- Kikuchi, K. and A.W. Hogan, 1978: Properties of diamond dust type ice crystals observed in summer season at Amundsen-Scott South Pole Station, Antarctica. *J. Meteorol. Soc. Jpn.*, **57**, 180-189.
- Korolev, A.V., G.A. Isaac and J. Hallett, 1999: Ice particle habits in Arctic clouds. *Geophys. Res. Letters*, **26**, 9, 1299-1302.
- Lawson, R.P., B.A. Baker, C.G. Schmitt and T.L. Jensen, 2001: An overview of microphysical properties of Arctic clouds observed in May and July during FIRE.ACE. *J. Geophys. Res.*, **106**, 14,989-15,014.
- Magono, C., and C. W. Lee, 1966: Meteorological classification of natural snow crystals. *J. Fac. Sci.*, Hokkaido University, **4**, No. 2.
- Mahesh, A., V. P. Walden, and S. G. Warren, 2001: Ground-based infrared remote sensing of cloud properties over the Antarctic Plateau. *J. Appl. Meteorol.*, **40**, 1279 – 1294.
- Orikasa, N. and M. Murakami, 1997: A new version of hydrometeor videoprobe for cirrus cloud observations. *J. of Meteor. Soc. of Japan*, **75** (6), 1033-1039.
- Oshchepkov S., H. Isaka, J-F Gayet, A. Sinyuk, F. Auriol and S. Havemann, 2000: Microphysical properties of mixed-phase and ice clouds retrieved from in situ airborne Polar Nephelometer measurements. *Geophys. Res. Letters*, **27**, 2, 209-212.
- Ohtake, T. and T. Yogi, 1979: Winter ice crystals at South Pole. *Antarct. J. U.S.*, **14**, 201-203.
- Ohtake, T. and M. Inoue, 1980: Formation mechanism of ice crystal precipitation in the Antarctic atmosphere. *8th International Conference on Cloud Physics*, 221-224.

Pruppacher, H.R., and J.D. Klett, 1997: Microphysics of Clouds and Precipitation, D. Reidel Publishing Company, 2<sup>nd</sup> Edition.

Sassen, K., J.M. Comstock, Z. Wang and G. Mace, 2001: Cloud and aerosol research capabilities at FARS: the Facility for Atmospheric Remote Sensing. *Bull. Of Amer. Meteorol. Soc.*, **82**, 1119-1138.

Shimizu, H., 1963: 'Long prism' crystals observed in precipitation in Antarctica. *J. Met. Soc. Japan*, **41**, 305-307.

Smiley, V.N., B.M. Whitcomb, B.M. Morley and J.A. Wharburton, 1980: Lidar determinations of atmospheric ice crystal layers at South Pole during clear-sky precipitation. *J. Appl. Meteorol.*, **19**, 1074-1090.

Tape, W., 1994: Atmospheric halos. *Antarctic Research Series*, **64**, American Geophysical Union, Washington, D.C., 143 pp.

Warren, S. G., 1996: Antarctica, in *Encyclopedia of Climate and Weather*. Oxford University Press, Oxford, 32 – 39.

**Acknowledgments:** This research was sponsored by the National Science Foundation under Grant No. OPP-9909593.